# Contrast and decay of cathodoluminescence from phosphor particles in a scanning electron microscope

Daniel den Engelsen, Paul G. Harris, Terry G. Ireland *, George R. Fern, Jack Silver

Centre for Phosphor and Display Materials, Wolfson Centre for Materials Processing, Brunel University London, Uxbridge, Middlesex UB8 3PH, UK

## ABSTRACT

Cathodoluminescence (CL) studies are reported on phosphors in a field emission scanning electron microscope (FESEM). ZnO: Zn and other luminescent powders manifest a bright ring around the periphery of the particles: this ring enhances the contrast. Additionally, particles resting on top of others are substantially brighter than underlying ones. These phenomena are explained in terms of the combined effects of electrons backscattered out of the particles, together with light absorption by the substrate. The contrast is found to be a function of the particle size and the energy of the primary electrons. Some phosphor materials exhibit a pronounced comet-like structure at high scan rates in a CL-image, because the particle continues to emit light after the electron beam has moved to a position without phosphor material. Image analysis has been used to study the loss of brightness along the tail and hence to determine the decay time of the materials. The effect of phosphor saturation on the determination of decay times by CL-microscopy was also investigated.

© 2015 Elsevier B.V. All rights reserved.

## 1. Introduction

The recording of cathodoluminescence (CL) is a standard technique in many scanning electron microscopes (SEM). A CL-micrograph from a SEM provides additional information on materials that are cathodoluminescent [1]. SEMs that are equipped with a photomultiplier tube can only record a panchromatic CL-image, while microscopes that have an additional monochromator can also record spectra. Important applications of CL-microscopy are in the field of mineralogy, studies of defects in luminescent crystalline materials and characterisation of nanostructures [2–5]. Although CL-microscopy in an SEM has been in use for more than 40 years, reports on CL-studies of phosphor powders are scarce [3,6].

Poelman and Smet have recently published results on time resolved CL spectroscopy of phosphor particles by blanking the electron beam of a SEM [6]. With this technique it is possible to investigate the decay behaviour of individual phosphor particles. Recently we have shown that the decay of CL from $Y_2O_3$:$Eu^{3+}$ particles can be derived from CL-micrographs with image analysis software [7]. Besides time dependent phenomena a CL-image shows other interesting static features such as contrast of particles. Like secondary electron (SE) micrographs, CL-images may show bright edges around the periphery of particles: this is contrast enhancement.

Fig. 1(A and B) are secondary electron (SE) and CL-micrographs respectively of ZnO:Zn particles recorded at a primary beam voltage of 10 kV. Both figures show bright edges or contrast enhancement of the phosphor particles. Bright edges in SE-micrographs of grainy material including phosphor powders are rather common: e.g. $SnO_2$ particles annealed at 1300 °C show bright edges in the SE-micrographs reported by Meastre et al. [4], while some $Y_3Al_5O_{12}$:$Tb^{3+}$ particles in a micrograph shown in the Phosphor Handbook also demonstrate bright edges [8].

In the SE micrographs of references [4] and [8] the particles with the bright edges sit on top of other particles. Particles that are situated deeper in the layer usually do not have bright edges. The same tendency can be observed in Fig. 1(A and B) the particles that adhere directly to the carbon substrate do not show bright edges. In the CL-micrograph this effect is even clearer than in the SE-micrograph.

The fact that the bright edges are observed in the phosphor particles in both the SE- and CL-micrographs is strong evidence that they arise from a common cause. The conventional explanation of particles with bright edges in SE micrographs is the location of the interaction volume in the particle: the closer the interaction volume is to the surface of the particle, the more SEs can escape and thus, the brighter the pixel(s) on the monitor screen. This is what Reimer called "surface-tilt" contrast [9]. This surface tilt explanation may be satisfactory for isolated particles; however, in phosphor layers with many particles there must be additional effects to explain that especially top-layer particles have bright edges, whereas deep-laying particles have not (or have much less).
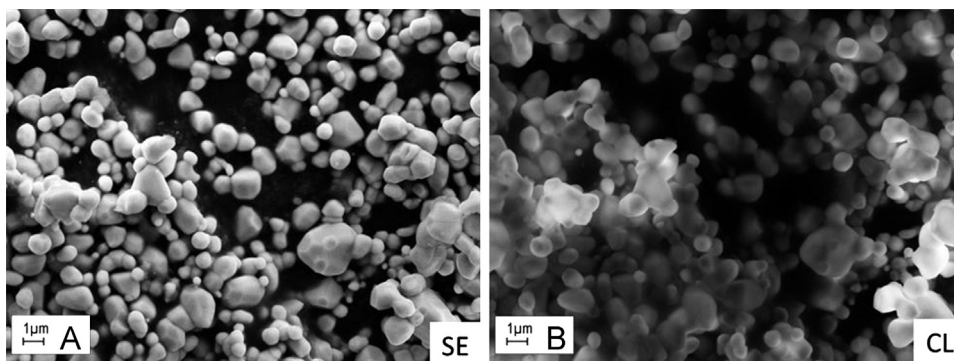
**Fig. 1.** (A) SE micrograph of ZnO:Zn at 10 kV. (B) CL micrograph of same area of ZnO:Zn at 10 kV ZnO:Zn powder is deposited on carbon substrate.

This additional reasoning could be the electric shielding of the top layer, which prevents complete extraction of SEs from deeper layers. However, this only explains attenuation of the SE-signals from both central and edge areas of particles; it does not rule out bright(er) edges of deeper particles. In other words, the conventional theory explaining the presence of bright edges is incomplete for SEs, nor can it explain the bright edges in a CL-micrograph, because the emission of SEs and CL arises from different physical processes. Furthermore, many phosphor materials are believed to have surface dead layers (due to unstable chemistry/contamination) and so, one might rather expect the edges to be dimmer in a CL-micrograph instead of brighter. Since there is no adequate explanation of the bright edges in CL- and SE-micrographs of phosphor particles, we have started an investigation with the objective of explaining this phenomenon as shown in Fig. 1(A). A second objective of this investigation is studying decay behaviour of phosphor particles in a SEM without beam blanking.

## 2. Materials and methods

### 2.1. Field emission scanning electron microscope

Fig. 2 shows schematically the geometry of the Zeiss Supra 35VP field emission scanning electron microscope (FESEM) used in this work. The system is equipped with four detector systems. The first is an Everhart-Thornley (ET) SE-detector, which collects primarily SEs, although some backscattered electrons (BSEs) may also contribute. There is also an in-lens SE-detector, for use when a very short working distance is required, and this detects only SEs. An annular (retractable) Robinson™ solid state BSE detector is mounted immediately above the sample. The microscope has the facility to operate in high pressures ( < 133 Pa) to facilitate imaging of specimens that charge under the beam. It is not possible to operate the ET SE-detector at high pressures and so an additional detector is fitted. This operates by using a photomultiplier (PM) tube to detect the fluorescence generated when low-energy SEs, emitted from the surface (under bombardment from the primary electron beam), excite the gas (nitrogen) in the chamber. If this detector is used under high vacuum conditions, then these signals are absent, and it is capable of generating high quality CL-images from suitable phosphor materials. The Cl-images produced in the Zeiss SEM are panchromatic. The response time of the PM tube is in the nanoseconds range; so, its effect on decay times in the micro- and milliseconds range can be neglected.

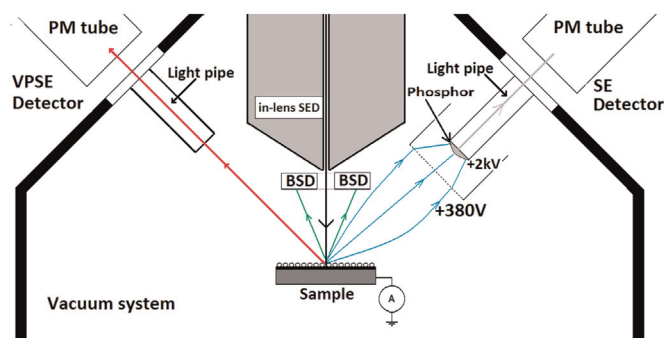Image analysis of the panchromatic CL-micrographs was performed using ImageJ (Public Domain) software.



**Fig. 2.** Schematic of the Zeiss Supra 35VP instrument.

### 2.2. Materials

Micrometre sized ZnO:Zn phosphor was obtained from Kasei Optonix, Japan and used without further treatment. The particle size of ZnO:Zn ranged from 0.4 to 1.5 μm. Nanometre monosized $Y_2O_3$:$Eu^{3+}$ has been synthesised in this laboratory. The synthesis has been described in detail in our previous work [10]; the average size was 330 nm. Commercial $Y_2O_3$:$Eu^{3+}$, $Y_2SiO_5$:$Tb^{3+}$ and $Gd_2O_2S$:$Tb^{3+}$ samples (micrometre sized) were obtained from Nichia, Japan. The concentration of the rare-earth dopants was 2 at% $Zn_2SiO_2$:$Mn^{2+}$ was supplied by Sylvania, USA. Finally, $InBO_3$:$Tb^{3+}$ and $SrGa_2S_4$:$Eu^{2+}$ were obtained from Phosphor Technology Ltd., UK. All commercial samples were analysed without additional purification and treatment.

Two types of substrates were used in this work, conductive graphite loaded pads and aluminium stubs. The graphite loaded pads were obtained from Agar Scientific and were slightly sticky. Phosphor powder was deposited either by a dusting technique or by dispensing a diluted phosphor suspension in ethanol. In the first case layers with 1–5 particles on top of each other were obtained, in the second case isolated particles could be deposited. In the case of aluminium substrates phosphor was applied by the alcohol dispensing technique.

## 3. Results and discussion

### 3.1. Contrast

Fig. 3 shows another micrograph of ZnO:Zn (at a higher magnification than those presented in Fig. 1 where the contrast enhancement of particles that sit on top of other is apparent. Those particles have bright edges, while the centre areas are darker. It is assumed that the effect of the backscattered electrons (BSEs) in particle clusters as shown in Fig. 3 is paramount. Before considering the effect of SEs and BSEs in particle clusters, the
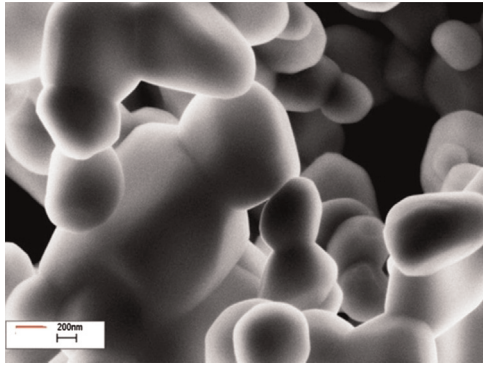
**Fig. 3.** CL-micrograph of ZnO:Zn at 10 keV.

geometrical effects that determine the contrast of a single particle will be described. The increase of the SE- and BSE-coefficients as a function of the angle incidence has been well described in the literature [11,12]

In Fig. 4 the left hand side shows the generation of SEs when a single particle is hit by primary electrons (PEs), whilst the right hand side illustrates the behaviour of BSEs. The number of both SEs and BSEs increases at oblique incidence. The enhancement of SE-emission is attributed to the close location of the interaction volume to the surface at $\varphi > 0°$. Fig. 4 shows that the distribution of scattering angles of the BSEs gets narrower when $\varphi > 0°$.

When the interaction volume is of the same dimension as or larger than the particle, the surface tilt contrast will largely disappear: this will be considered in more detail in Section 3.3. The size of the interaction volume depicted in Fig. 4 depends on the energy of the primary electrons, the atomic number and the density of the particle. In this work we focus on phosphor materials such as ZnO:Zn and $Y_2O_3:Eu^{3+}$. Although the interaction volume is not exactly spherical, its diameter can be represented by the maximum penetration depth of the primary electrons.

The penetration depth of electrons in ZnO:Zn as a function of primary energy (anode voltage) is represented in Fig. 5(A). The formula of Kanaya and Okayama [13] has been used to calculate this electron penetration curve, because it is close to the result of the simulation of the electron density plot with the Casino software package [14]. The interaction volume of the PEs at 10 kV is smaller than the average particle size, $d_{50}$, of ZnO:Zn, which justifies the relative sizes of the radii of the particle and the interaction volume in Fig. 4, which also shows that when $\varphi > 45°$, the BSEs are mostly heading for the substrate. If the substrate does not reflect these BSEs, it is to be expected that a BSE-detector positioned above the sample will show a particle with fainter edges,
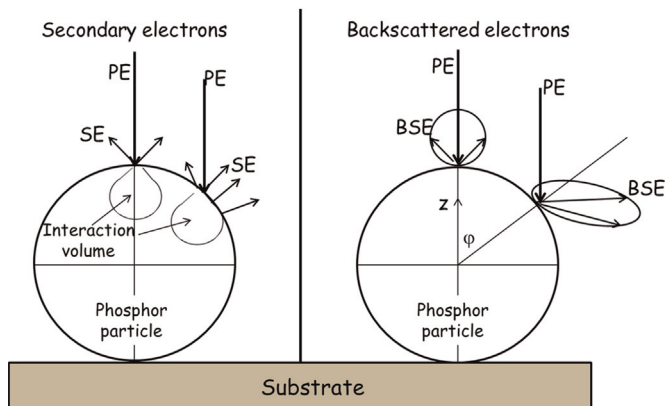


**Fig. 4.** Generation of secondary and backscattered electrons at a spherical particle, bombarded with primary electrons (PE). $\varphi$ is the angle of incidence of the PEs.

because less BSEs will be detected when the primary beam is at the edge.

The escape probability of a photon from a phosphor particle is determined by the angle between its propagation direction and the normal to the surface. If this angle is larger than the critical angle, being 30° for ZnO:Zn, the photon will be totally internally reflected. In a phosphor particle a photon can usually escape after experiencing one or more internal reflections. This effect may explain the observation that there is less directionality in the CL- than the SE-images; the latter are brighter on the side facing the SE-detector. Multiple reflections inside the particles average out any advantage of being on the side of the particle closest to the CL-detector. If in a spherical particle the photons are generated in the centre, all photons will escape directly. Off-centre generated photons may experience internal reflections. When the primary electron beam is on the edge of a spherical particle, most photons will be created closer to the surface. That will not affect the escape probability dramatically. However, due to the fact that the number of BSEs increases at the edge, the number of primaries entering the particle decreases so that the total number of photons at the edge will be less. In other words, for an isolated, luminescent-active particle it is to be expected that the edge will be fainter in a CL-micrograph. So, unlike the SE-micrograph, the CL-micrograph of an isolated phosphor particle will not show an enhanced surface tilt contrast.

The fate of various types of BSEs in a cluster of particles is shown in Fig. 6. In Fig. 6, type 1 primary electrons (PEs), hitting particle A in the centre, create BSEs that will not impinge on neighbouring particles, while type 2 PEs, hitting particle A at the edge, generate BSEs that will largely land on particle B and a few may land on D. These BSEs have sufficient energy to penetrate B, create an interaction volume and generate photons. Although the PE-beam is still at the edge of particle A, the instantaneous CL comes partly from B. In Fig. 6, type 3 PEs hitting particle E in the centre will also generate BSEs that can hit particle B. The back-scatter coefficient of type 1 PEs hitting particle A in the centre is about 20% (in the case of ZnO:Zn), whereas the backscatter coefficient of type 2 PEs is about 40%. This increase of the backscatter coefficient is caused by the non-normal angle of incidence of type 2 PEs.

Let us assume that type 1 PEs generates a CL-flux of 80 units and that type 2 PEs generates a CL-flux of 60 units. To this latter flux we must add the photons generated by BSEs in particle B. In the maximum case this would be 40 units. In reality, it will be a bit less, because some BSEs have a lower energy than the original PEs. So, a cluster of phosphor particles may have the geometric conditions to enhance a surface contrast in a CL micrograph: i.e. (bright) edges may become brighter. The electron bombardment of particle B, when the electron beam is still on A, also indicates that especially top layer particles will get bright edges, because of the large quantity of BSEs that are channelled downward. This analysis also explains why the top layer of particles in a SE-micrograph shows enhanced surface contrast.

With reference to the previous Figs. 1 and 3, which illustrate the foregoing consideration: bright edges are observed especially in the top particles. Additional experiments with wires of gold (Au), tin (Sn) and aluminium (Al) were made to verify the explanation. The wires were positioned on top of a layer of ZnO:Zn particles. From the aforementioned Fig. 7 shows the effect of BSEs from Au and Al wires stretched across the phosphor layer. Of course, Au and Al do not generate CL and the light observed at the edge of the Au wire is due to BSEs (from the Au wire) hitting the adjacent phosphor. The bright edge is due to higher backscattering coefficients at shallow incidence and also because the BSEs are directed onto the phosphor rather than away from the surface. The diagram at the left side of Fig. 7 represents the grey scale of the Au
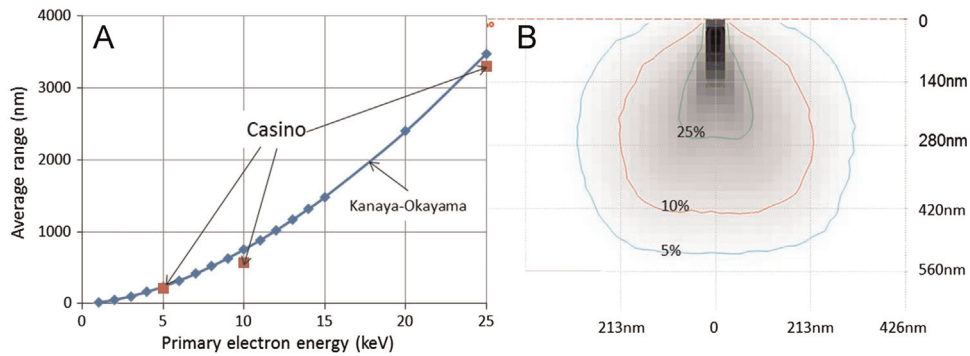
**Fig. 5.** (A) Average penetration depth for ZnO:Zn as a function of primary electron energy. (B) Simulated electron density plot (Casino) of PEs at 10 keV in ZnO:Zn. The average range in (A) is the average of the ranges in the normal and lateral direction shown in (B).
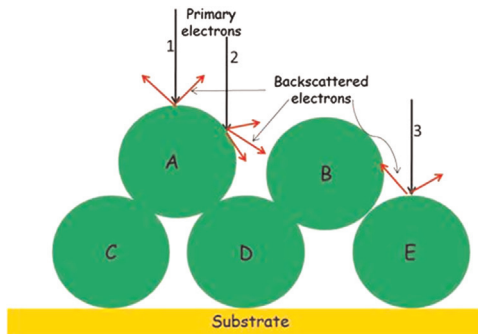


**Fig. 6.** Backscattered electrons in a cluster of particles.

wire along the arrow indicated at the right side. The corresponding light that apparently is coming from an Al wire on top of a layer of ZnO:Zn particles is less, because the backscatter coefficient of Al is less than that of Au.

### 3.2. Decay

Since a CL-micrograph is represented in shades of grey, it is also called panchromatic. The grey shades $G_{ij}$ in a CL-graph, where $i$ and $j$ indicate a pixel in the ith row and jth column, can be written as:

$$G_{ij} = (1 - \eta_{ij})B_{ij} + \sum_k f_{ij}^{\ k}(1 - \eta_{ij}^{\ k})B_{ij}^{\ k} \quad (1)$$

where $\eta_{ij}$ is the backscatter coefficient at pixel $ij$, $f_{ij}^{\ k}$ is the fraction of BSEs going from $ij$ to a neighbouring pixel $k$ and $\eta_{ij}^{\ k}$ is the backscatter coefficient of second generation BSEs, starting at $ij$ and hitting another particle at pixel $k$. The quantity $B_{ij}$, being the grey value generated by the PEs at pixel $i,j$, is defined as

$$B_{ij} = V_{ij} \int P(\lambda)_{ij} s(\lambda) d\lambda \quad (2)$$

where $V_{ij}$ is the viewing factor of pixel $i,j$ to the optical detector. From this definition it follows that $V_{ij}$ also takes account of shadowing effects caused by other particles. $P(\lambda)_{ij}$ is the power distribution spectrum of the light generated at pixel $i,j$ and $s(\lambda)$ is the sensitivity of the photocathode of the photomultiplier. The integration is made between the minimum and maximum wavelengths of $s(\lambda)$. Eq. (2) indicates that the grey scale in a CL-micrograph is not equal to its luminance, because $P_{ij}$ is convoluted with s and not with the eye sensitivity function. The grey scale $G_{ij}$ is also a function of time, because of the decay of the fluorescence (or phosphorescence). If the decay time is more than 4 orders of magnitude smaller than the scan rate, there will no smearing effect visible in the CL-micrograph. For longer decay times, smearing will be visible. The Zeiss Supra FESEM is provided with scan rates of 1.7 s–0.12 ms per line and this defines the range of materials that can be studied. For weakly luminescent materials and/or the highest scan speeds the images can repeatedly be scanned and averaged to improve signal to noise.

Fig. 8 shows SE- and CL-micrographs of various phosphor particles. Fig. 8(A) is a SE-micrograph of a cluster of nanosized $Y_2O_3$:$Eu^{3+}$ particles and a single $Gd_2O_2S$:$Tb^{3+}$ particle on a carbon substrate, a graphite-loaded pad. Fig. 8(B) is a CL-micrograph of the same area. Fig. 8(C) is a SE-micrograph of $Y_2SiO_5$:$Tb^{3+}$ particles on a carbon substrate, while Fig. 8(D) is the CL-image of the area shown in Fig. 8(C). The SE-micrographs are sharp images and show details of the particles, whereas the CL-micrographs are smeared out. The reason for this blurring is the rather long decay times of $Y_2O_3$:$Eu^{3+}$, $Gd_2O_2S$:$Tb^{3+}$ and $Y_2SiO_5$:$Tb^{3+}$. In other words, smearing of CL-images offers the opportunity to measure decay times of CL-phosphors.

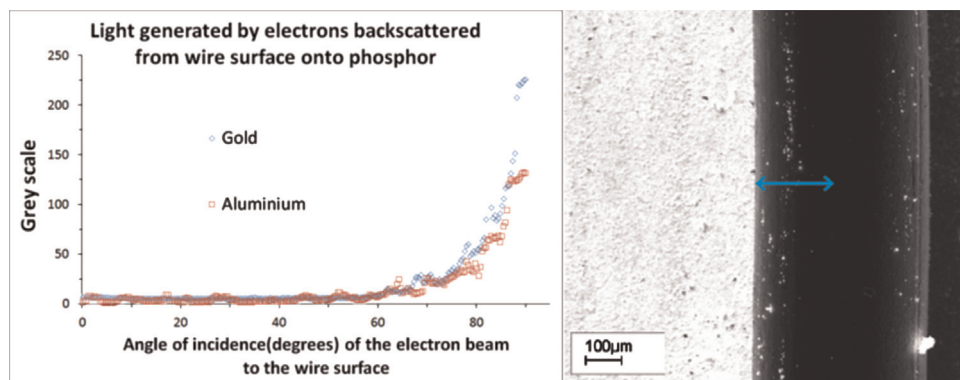The decay times can be determined by analysing the grey scales



**Fig. 7.** CL image of electron scattering from a gold wire. The detector is located to the left. The phosphor layer in this example is ZnO:Zn.
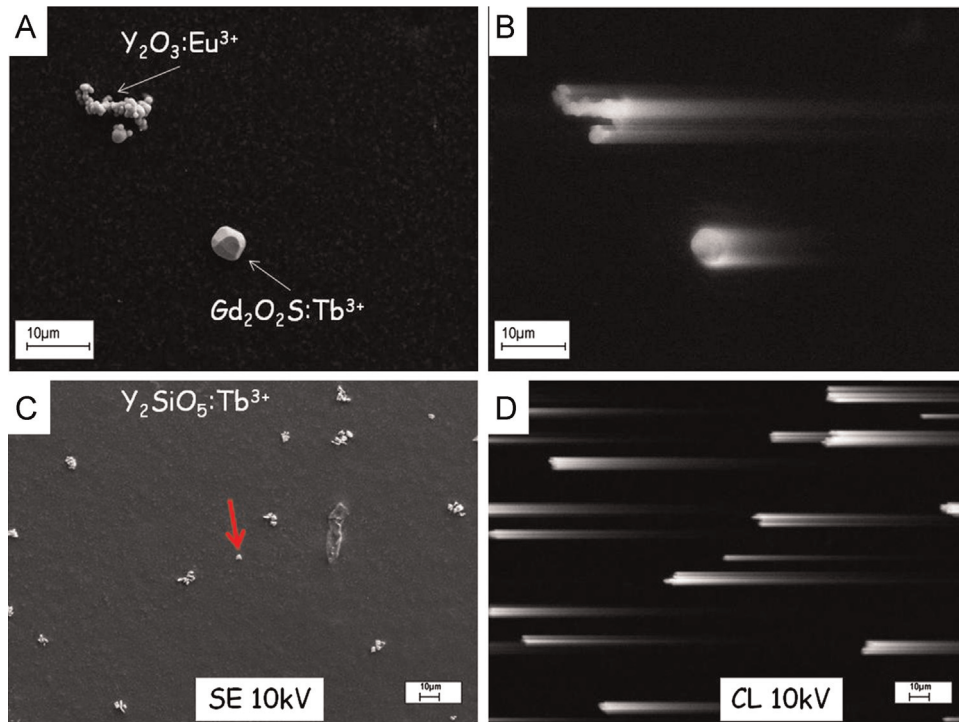
**Fig. 8.** (A) SE-micrograph of a cluster of $Y_2O_3$:$Eu^{3+}$ particles and a single $Gd_2O_2S$: $Tb^{3+}$ particle. (B) CL-micrograph of same area as shown in (A). (C) SE-micrograph of $Y_2SiO_5$:$Tb^{3+}$ particles. (D) CL-micrograph of same area as shown in (C). Primary electron energy 10 keV, scanning rate of 10.1 s/frame.

of comet-like structures as shown in Fig. 8(B and D). These analyses were made with the ImageJ software; an example is shown in Fig. 9 for $Y_2SiO_5$:$Tb^{3+}$. The comets shown in Fig. 8(B and D) are represented in spatial dimensions. From the known scanning speed of the electron beam in the FESEM and the number of pixels ($1024 \times 768$), length can be converted into time.

Fig. 9 shows two curves: the noisy curve has been determined with ImageJ from the CL-micrograph, whilst the smooth curve is a fit of $G$ to the experimental data in terms of one exponential function:

$$G = G_{max}\, e^{-t/\tau} + BG \qquad (3)$$

where $G_{max}$ is the measured maximum value of the grey scale (maximum is 256 in 8-bits representation), t indicates the time, being 0 when $G = G_{max}$, $\tau$ is the time constant, being the 1/e-value of the decay time ($\tau_{1/e}$), and BG is the background correction. This latter correction depends on the gain setting of the photo-multiplier tube that amplifies the weak CL from individual phosphor particles in the FESEM chamber.

The $Y_2SiO_5$:$Tb^{3+}$ particle, from which the grey scale curve of

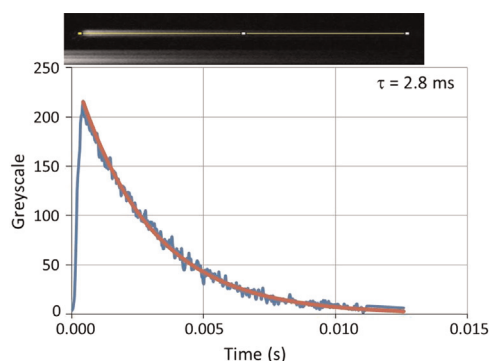Fig. 9 is derived, is indicated in Fig. 8(C) by the arrow. Fig. 9 thus shows the advantage of this technique: the determination of the decay time of individual nanosized particles. It can be seen in Fig. 8(B) that in the case of a cluster of particles, it will be impossible to determine $G_{max}$ or the start time unambiguously. In that case the magnification needs to be lowered to enable a more accurate determination of the start time. As explained afore, the CL detector in the Zeiss FESEM is a photomultiplier tube. So, the CL-images are panchromatic. The decay times determined with this technique are therefore "overall decay times" and cannot be compared to spectral selective decay times.

We have measured the overall decay times of various commercial phosphors to get an impression of the range of decay times that can be measured by this method. The results are shown in Table 1. The shortest overall decay time determined was 2.3 μs for $SrGa_2S_4$:$Eu^{2+}$. In this case, the fastest scan rate of the SEM (90 ms per frame) was used. At this high scan rate it was necessary to use frame averaging to achieve good signal to noise ratios. From our data we conclude that the minimum decay time that can be determined with the FESEM used in this work is $\sim 1$ μs. The longest decay time that could be determined is about 0.1 s; so, the



**Fig. 9.** Grey scale of Cl-micrograph (10 keV) versus time for $Y_2SiO_5$:$Tb^{3+}$ particle. The single particle comet was used to construct the diagram.

**Table 1**
Overall decay times determined from CL-micrographs

| Material source | $\tau_{1/e}$ (ms) | | Ref. |
|---|---|---|---|
| | This work | Literature | |
| $Y_2O_3$:$Eu^{3+}$ (Nichia) | 1.2 | 1.2, 1.12, 1.1 | [15,16,17] |
| $Y_2O_3$:$Eu^{3+}$ (Brunel) | 1.0 | 1.06 | [7] |
| $Zn_2SiO_4$:$Mn^{2+}$ (Sylvania) | 3.3 | 8[*] | [18] |
| $InBO_3$:$Tb^{3+}$ (PT) | 3.2 | 2.1 | [19] |
| $Y_2SiO_5$:$Tb^{3+}$ (Nichia) | 2.8 | 3.2 | [20] |
| $SrGa_2S_4$:$Eu^{2+}$ (PT) | 0.0023 | $\sim 0.001$ | [21] |
| $Gd_2O_2S$:$Tb^{3+}$ (Nichia) | 0.56 | 0.558 | [22] |

[*] This value refers to $\tau_{10\%}$. The $\tau_{10\%}$ of the $Zn_2SiO_4$:Mn sample in our work is 7.6 ms, which indicates that the Mn-doping is $\sim 5\%$ according to the information in [18].
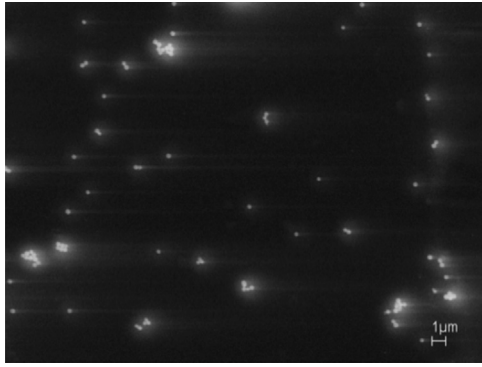
**Fig. 10.** CL micrograph of monosized $Y_2O_3$:Eu spheres on Al substrate. Beam energy 10 keV, scan rate 5.1 s/frame.

range of decay times that can be determined with this method is about 5 decades. The agreement between the overall decay times determined in this work with those published in the literature is satisfactory.

We also tried to measure decay times of phosphors deposited on Al substrates. Fig. 10 is a CL-micrograph of monosized $Y_2O_3$:$Eu^{3+}$ (2% $Eu^{3+}$) spheres with a diameter of about 300 nm on an Al substrate. Unlike the CL micrographs of phosphors on the graphite-loaded pads, the CL micrograph shown in Fig. 10 shows a noticeable halo effect surrounding each particle that is of similar intensity to the comet tails. What appears to be happening is that a fraction of the electrons striking the substrate immediately around each phosphor particle are backscattered onto the particle, causing it to emit light.

The reason that we can see this clearer from the aluminium substrate than from the graphite-loaded polymer substrate is the much larger backscatter coefficient of aluminium $\sim 13\%$ at 10 keV, as compared to that on graphite-loaded polymers of $\sim 2.2\%$ at 10 keV. These backscatter coefficients were estimated using the Casino software package [14]. A similar picture to that in Fig. 10 has been reported by us previously [7]. Although it is possible to evaluate decay times from CL micrographs as presented in Fig. 10,

the accuracy is reduced and the preferred measuring method is to use substrates with low backscatter coefficients, such as graphite-loaded pads or Formvar-coated TEM grids.

### 3.3. Discussion

In the discussion of Fig. 4 in Section 3.1 no attention was paid to the ratio $\alpha$ between the diameter of the particle size and the diameter of the interaction volume. This ratio $\alpha$ is

$$\alpha = \frac{d_{50}}{R} \tag{4}$$

where $d_{50}$ is the average diameter of the particles and $R$ is the electron range, depicted in Fig. 5(A) for ZnO:Zn. Fig. 11 shows some CL-micrographs of ZnO:Zn at different energies of the PEs. The contrast represented in Fig. 11(D) is defined as the grey value at the edge of a particle divided by the grey value in the centre: so, contrast=1 is equivalent to no bright edge. The contrast represented in Fig. 11(D) corresponds to areas where the brightness is rather large. At 25 keV $R$ is 3.4 times larger than $d_{50}$; this reduces the resolution of the CL-micrograph and at that condition no bright edges are observed.

At 5 keV, the range is about 4 times smaller than the particle diameter, yielding a good resolution and a contrast of 1.6. Other examples of the effect of $\alpha$ on contrast are depicted in Fig. 12, being SE and CL micrographs of $Y_2O_3$:$Eu^{3+}$ and ZnS:Cu,Cl at 10 keV primary beam energy. At a beam energy of 10 keV the diameters of the interaction volume in $Y_2O_3$:Eu and ZnS:Cu,CL are 1.0 and 1.3 µm respectively: for $Y_2O_3$:$Eu^{3+}$ it is much larger than the particle size, whereas for ZnS:Cu,Cl it is much smaller. Expressed in the parameter $\alpha$:$\alpha$ at 10 keV is 0.25 and 17 for $Y_2O_3$:Eu and ZnS:Cu,Cl respectively. These phosphors do not show bright edges, neither in the SE-micrographs, nor in the CL-micrographs. In other words: for $\alpha > 10$ the contrast is also approaching 1. So, we may conclude that the sweet spot for contrast enhancement, or bright edges, is $0.4 < \alpha < 8$.

Particles and clusters of particles in Fig. 12(A, B and D) sitting on top of others are generally brighter due to the effects explained
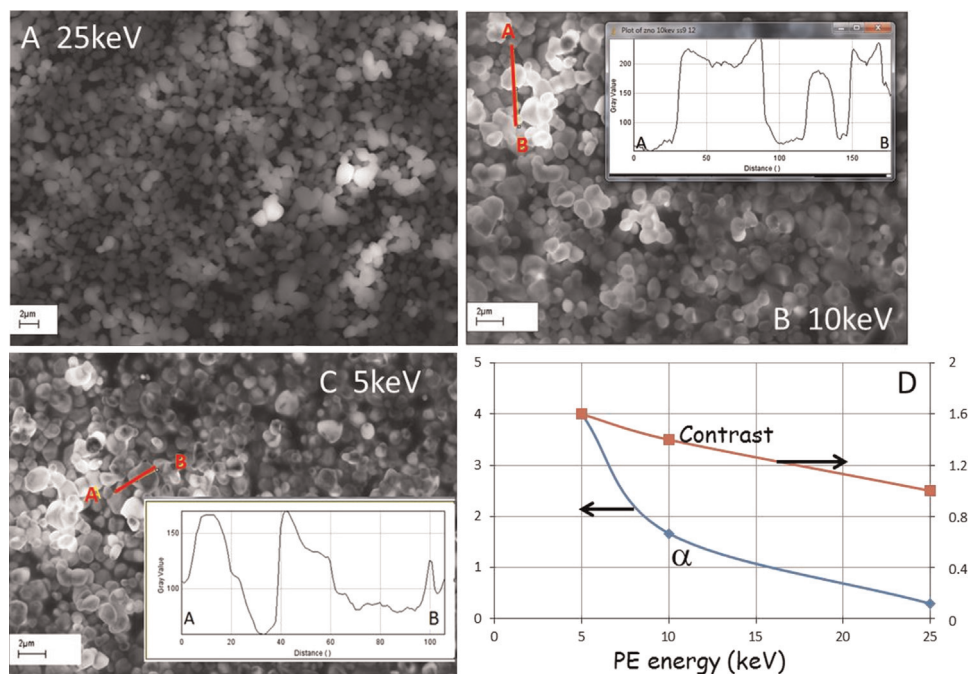


**Fig. 11.** (A–C) CL-micrographs of ZnO:Zn at 25, 10 and 5 keV respectively. (D) contrast and $\alpha$ as a function of PE-energy. The inserts in (B and C) show variations in grey value along the lines AB.
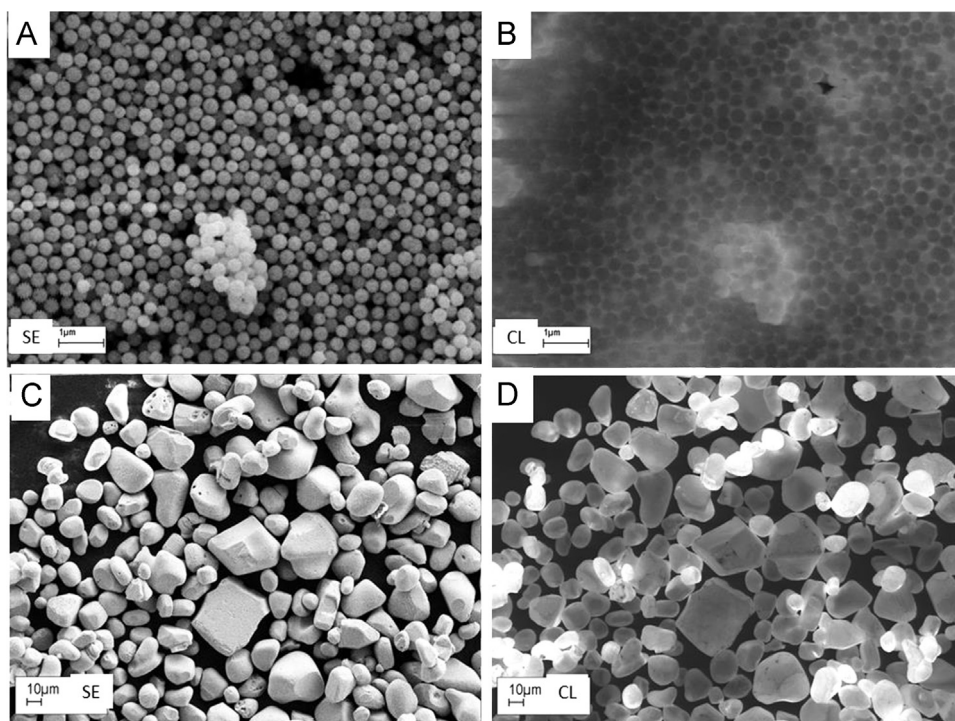
**Fig. 12.** (A and B) Micrographs of the same area of monosized $Y_2O_3$:$Eu^{3+}$ at 10 keV on ITO substrate. (C and D) Micrographs of the same area of ZnS:Cu,Cl at 10 keV on C-substrate. (A and C) SE-micrographs, (B and D) CL-micrographs.

in Figs. 6 and 7. Fig. 12(B) is blurred because of the long decay time of the luminescence. The brightness increase of particles on top of others is particularly striking in Fig. 12(D). Due to the light absorbing substrate an additional effect may enhance the brightness difference between top particles and particles touching the substrate. This effect is depicted in Fig. 13. In particle 1 a substantial number of the emitted photons is scattered by other particles and may reach the detector, whereas in particle 2 a noticeable number of emitted photons is absorbed in the substrate (carbon).

Apart from differences in contrast, Fig. 12 shows areas with different brightness. It is assumed that areas with high brightness are caused by charging of particles sitting on top of a lower layer. Charging will certainly occur in $Y_2O_3$:$Eu^{3+}$ and ZnS:Cu,Cl because of the low conductivity of these materials. The appearance of bright-particle clusters in Fig. 12(A and B) and bright particles in (D) can be explained by negative charging. ZnO:Zn has a rather high conductivity; however, if the contact areas between upper and lower particles are small, then charging cannot be excluded. If these top particles are negatively charged, low energy BSEs will be deflected to neighbouring particles.

In our recent study of the CL from nanosized $Y_2O_3$:$Eu^{3+}$ particles it has been shown that in a FESEM, which has a small electron spot, phosphors particles are readily saturated[7]. This
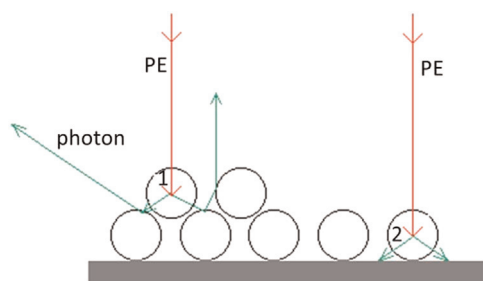


**Fig. 13.** Different light output of particle 1 and particle 2. More light is absorbed for particle 2.

means that the efficiency of the CL becomes much lower: this does not moot a principle problem. However, since saturation may work out differently for various transitions in the spectrum, the decay behaviour and the dominant colour of the fluorescence may change. The first consequence of saturation can be studied with the procedure explained in Section 3.2. The effect of saturation on the determination of the overall decay time for $Y_2O_3$:$Eu^{3+}$ with 1% $Eu^{3+}$ is shown in Fig. 14.

The grey scale of the comet shown in Fig. 14(A) is represented in Fig. 14(B) by the noisy curve. This curve cannot be represented by one exponential, but rather by two:

$$G = G_f \, e^{-t/\tau_f} + G_s \, e^{-t/\tau_s} + BG \qquad (5)$$

where $G_f$ and $G_s$ are the pre-exponential factors for the fast and slow decay processes, respectively, $\tau_f$ and $\tau_s$ are the corresponding time constants. The values for $\tau_f$ and $\tau_s$ are 0.1 and 1.2 ms respectively. The time constant for the slow process can be ascribed to the strongest peak in the CL spectrum of $Y_2O_3$:$Eu^{3+}$, viz. the $^5D_0 \rightarrow {}^7F_2$ ($C_2$) transition at 611 nm, whereas the fast decay process can be attributed to the $^5D_1 \rightarrow {}^7F_1$ ($C_2$) transition at 533 nm. The first spectral transition at 611 nm saturates more quickly than the second at 533 nm[7]. Thus by studying the exponential tail at a range of beam currents (below and above the point at which one transition saturates) the decay time constants of different spectral transitions can be studied. The value for $\tau_s$ agrees with the data for the $^5D_0 \rightarrow {}^7F_2$ ($C_2$) transition at 611 nm, while the value for $\tau_f$ corresponds favourably with 0.09 ms for the $^5D_1 \rightarrow {}^7F_1$ ($C_2$) transition at 533 nm[7].

## 4. Conclusions

We have described the contrast enhancement in SE- and CL-images of phosphor powders recorded with a FESEM. Both sets of micrographs can show the presence of bright edges of particles sitting on top of other particles. This behaviour can be explained
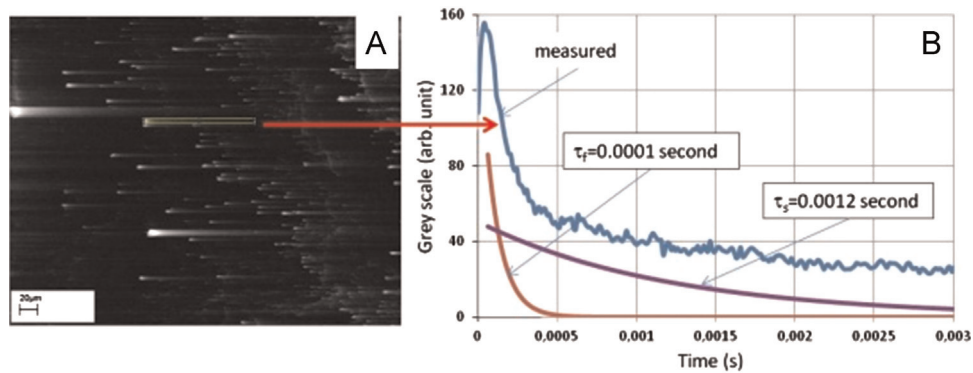
**Fig. 14.** (A) CL-image of $Y_2O_3$:$Eu^{3+}$ with 1% $Eu^{3+}$ at 10 keV. (B) Grey scale of indicated cluster (noisy curve).

by BSEs leaving the first particle and exciting SEs or photons in particles that are in their immediate vicinity, particularly just below them. In the case of single particles, contrast enhancement in the CL-micrographs does not occur, whereas it may appear in SE-micrographs, in this case due to enhanced SE emission when the beam strikes the edge of the particle.

CL-microscopy is found to be well suited for measuring overall decay times in the range between 1 µs and 0.1 s for individual phosphor particles, which may have micrometre or nanometre dimensions. No additional investments are needed to make these measurements with a (FE)SEM that is equipped with a CL-sensor. Substrates with low backscatter coefficients, e.g. carbon or better still formvar coated TEM grids, are recommended for this measuring method, to avoid complications due to excitation by backscattered electrons from the substrate.

The effect of phosphor saturation is a special point of attention: in the case of a fluorescence spectrum with different types of spectral transitions the decay curves measured with a FESEM are sums of the emissions from possible transitions present. By working at a wide range of beam currents, above and below the saturation point of the slower transitions, facilitates the determination of time constants of different transitions from the data. If the fluorescence in the FESEM is spectrally resolved, direct assignment of decay curves to spectral transitions is possible.

We suggest that our new measuring method of analysing the temporal information, panchromatic or spectrally resolved, in CL-micrographs is facile and can be applied in studies of individual micro and nano particles.

## Acknowledgements

## References

[1] B.G. Yacobi, D.B. Holt, Cathodoluminescence scanning electron microscopy of semiconductors, J. Appl. Phys. 59 (1986) R1–R24.
[2] J. Götze, Potential of cathodoluminescence (CL) microscopy and spectroscopy for the analysis of minerals and materials, Anal. Bioanal. Chem. 374 (2002) 703–708.
[3] M.R. Phillips, Cathodoluminescence microscopy and spectroscopy of optoelectronic materials, Microchim. Acta 155 (2006) 51–58.
[4] D. Maestre, A. Cremades, J. Piqueras, Cathodoluminescence of defects in sintered tin oxide, J. Appl. Phys. 95 (2004) 3027–3030.
[5] B. Dierre, X. Yuan, T. Sekiguchi, Low-energy cathodoluminescence microscopy for the characterization of nanostructures, Sci. Technol. Adv. Mater. 11 (2010) 043001.
[6] D. Poelman, P.F. Smet, Time resolved microscopic cathodoluminescence spectroscopy for phosphor research, Physica B 439 (2014) 35–40.
[7] D. den Engelsen, P.G. Harris, T.G. Ireland, J. Silver, Cathodoluminescence of nanocrystalline $Y_2O_3$:$Eu^{3+}$ with various $Eu^{3+}$ concentratio, ECS J. Solid State Sci. Technol. 4 (2015) R1–R9.
[8] K. Ohno, Phosphors for Cathode-Ray Tubes, in: W. Yen, S. Shionoya, H. Yamamoto (Eds.), Phosphor Handbook: The CRC Press Laser and Optical Science and Technology series, CRC Press, Boca Raton, 2007, p. 596.
[9] L. Reimer, Scanning Electron Microscopy, second ed, Springer, Heidelberg (1998), p. 210.
[10] D. den Engelsen, P.G. Harris, T.G. Ireland, R. Withnall, J. Silver, Cathodoluminescence of powder layers of nanometer-sized $Y_2O_3$:Eu and micrometer-sized ZnO:Zn phosphor particles, ECS J. Solid State Sci. Technol. 2 (2013) R201–R207.
[11] E.H. Darlington, V.E. Cosslett, Backscattering of 0.5–10 keV electrons from solid targets, J. Phys. D: Appl. Phys. 5 (1972) 1969–1981.
[12] H. Niedrig, Electron backscattering from thin films, J. Appl. Phys. 53 (1982) R15–R49.
[13] K. Kanaya, S. Okayama, Penetration and energy-loss theory of electrons in solid targets, J. Phys. D: Appl. Phys. 5 (1971) 43–58.
[14] D. Drouin, A.R. Couture, D. Joly, X. Tastet, V. Aimez, R. Gauvin, CASINO V2.42: a fast and easy-to-use modeling tool for scanning electron microscopy and microanalysis users, Scanning 29 (2007) 92–101.
[15] Y. Chung, S. Park, K. Jang, I. Kim, Y.I. Lee, H.J. Seo, Optical properties and crystal structure of $Eu^{3+}$-doped $Y_2O_3$ crystals prepared under different conditions and with different Metho, J. Korean Phys. Soc. 42 (2003) 543–548.
[16] D.R. Tallant, C.H. Seager, R.L. Simpson, Unusual persistence behavior in rare-earth-activated oxide phosphors, Extended Abstracts of The fifth International conference on the science and technology of display phosphors, November 8–10, San Diego, CA (1999) pp. 325–328.
[17] J. Thomes, C. Seager, D. Tallant, P. Holloway, Effects of MgO and $A1_2O_3$ coatings on $Y_2O_3$:Eu and $Y_2SiO_5$:Tb CL phosphors, Extended Abstracts of The sixth International conference on the science and technology of display phosphors, November 6–8, San Diego, CA, (2000) pp. 249–251.
[18] N. Taghavinia, G. Lerondel, H. Makino, A. Yamamoto, T. Yao, Y. Kawazoe, T. Goto, Nanocrystalline $Zn_2SiO_4$:$Mn^{2+}$ grown in oxidized porous silic, Nanotechnology 12 (2001) 547–551.
[19] Z.W. Chiu, T.H. Fang, Y.J. Hsiao, Optical characteristics of Tb-doped $InBO_3$ nanocrystals, J. Lumin. 132 (2012) 2608–2611.
[20] H. Jiao, N. Zhang, X. Jing, D. Jiao, Influence of rare earth elements (Sc, La, Gd and Lu) on the luminescent properties of green phosphor $Y_2SiO_5$:Ce,Tb, Opt. Mater. 29 (2007) 1023–1028.
[21] K.A. Talin, J.E. Dean, Jaskie, Field emission displays: a critical review, Solid-State Elect. 45 (2001) 963–976.
[22] A.G. Glendinning, S.G. Hunt, D.E. Bonnett, Measurement of the response of $Gd_2O_2S$:Tb phosphor to 6 MV X-rays, Phys. Med. Biol. 46 (2001) 517–530.